





Energy storage in magnetic textures driven by vorticity flow

Dalton Jones , Ji Zou , Shu Zhang , and Yaroslav Tserkovnyak

Department of Physics and Astronomy, University of California, Los Angeles, California 90095, USA

 (Received 30 March 2020; revised 15 July 2020; accepted 23 September 2020; published 28 October 2020)

An experimentally feasible energy-storage concept is formulated based on vorticity (hydro)dynamics within an easy-plane insulating magnet. The free energy associated with the magnetic winding texture is built up in a circular easy-plane magnetic structure by injecting a vorticity flow in the radial direction. The latter is accomplished by electrically induced spin-transfer torque, which pumps energy into the magnetic system in proportion to the vortex flux. The resultant magnetic metastable state with a finite winding number can be maintained indefinitely because the process of its relaxation via phase slips is exponentially suppressed when the temperature is brought well below the Curie temperature. We characterize the vorticity-current interaction underlying the energy-loading mechanism through its contribution to the effective electric inductance in the rf response. Our proposal may open an avenue for naturally powering spintronic circuits and nontraditional magnet-based neuromorphic networks.

DOI: [10.1103/PhysRevB.102.140411](https://doi.org/10.1103/PhysRevB.102.140411)

Introduction. The centerpiece of the global energy challenge today is a viable method for energy storage, whose key is to convert captured energy into forms that are convenient or economic for long-term storage. Commonly used forms of energy storage are based on chemical energy (lithium-ion batteries), gravitational energy (hydroelectric dam), thermal energy (molten salt), etc. Recent progress in the field of spintronics enables us to manipulate magnetic textures in numerous ways [1–3], which inspires the possibility of storing energy in the exchange energy associated with topological magnetic textures [4].

Here we propose a feasible scheme for energy storage in the topological magnetic winding texture of a magnetic insulator. The physical mechanism for charging or discharging is through the control of radial vorticity flows in a Corbino geometry. A “phase slip” in a spin superfluid [5] is known to reduce the phase winding of a one-dimensional system with XY order by 2π by sending a vortex across it. Vice versa, driving a vortex flow in the opposite direction will naturally build up the winding number and hence the magnetic exchange energy. Different from Ref. [4], where a locally induced spin Hall torque is used to produce spin winding of a one-dimensional magnetic loop, the present proposal is based on a quasi-two-dimensional annulus, where a spin-transfer torque is applied over the entire area of the magnetic film, in order to inject an isotropic radial vortex current. This vorticity flow is accomplished at elevated temperatures, where the magnetic system may be disordered with no XY order present, even locally. The topological protection of the induced winding is recovered when, after texturing the magnet by the vortex flow, we cool the system in order to prevent any parasitic phase slips.

Although our structure is limited in terms of energy density compared with the prevalent lithium-ion battery technology, our approach does have a few advantages. First, magnetic

systems are highly nonvolatile and durable. Magnetic textures protected by nontrivial topological numbers, such as domain walls, vortices, and skyrmions, have already been employed in memory and logic devices [6–9]. Energy can be stored over an extremely long timescale, with essentially no degradation in charging and discharging cycles. Second, magnetic batteries can be naturally incorporated into spintronic circuits [6,10–12], neuromorphic platforms [13–17], and quantum-information processing tasks based on insulating magnets [18–20], rendering coherent and low-dissipation operations based purely on spin dynamics. Third, common magnetic materials are environmentally friendly, and the development of magnetic batteries is another possible avenue leading to the goal of clean energy.

Central concept. To illustrate our concept, we consider the annulus structure depicted in Fig. 1. A thin-film easy-plane magnetic insulator is placed on top of a metal contact. The magnetic insulator can be ferro- or antiferromagnetic, with a vectorial order parameter $\mathbf{n}(\mathbf{r}, t)$ which fluctuates in both direction and magnitude. The in-plane texture is described by the spin-space azimuthal angle $\varphi(l, t)$, where l is the polar position. The metal annulus has a uniform magnetic order $\mathbf{M} = M\hat{\mathbf{z}}$.

We define the vorticity 3-current in $(2 + 1)$ dimensions within the thin-film magnetic insulator as

$$\mathcal{J}^\mu = \epsilon^{\mu\nu\rho} \hat{\mathbf{z}} \cdot (\partial_\nu \mathbf{n} \times \partial_\rho \mathbf{n}) / 2\pi, \quad (1)$$

which is carried by the magnetic texture [21]. Here $\epsilon^{\mu\nu\rho}$ is the Levi-Civita symbol (with the Einstein summation implied over the Greek indices $\mu = 0, 1, 2 \leftrightarrow t, x, y$). The current obeys a topological conservation law, $\partial_\mu \mathcal{J}^\mu = 0$. The total vortex number in the bulk Ω ,

$$\mathcal{N} = \int_\Omega dx dy \mathcal{J}^0 = \frac{1}{2\pi} \int_{\partial\Omega} d\vec{l} \mathbf{n}_\parallel^2 \vec{\nabla} \varphi, \quad (2)$$

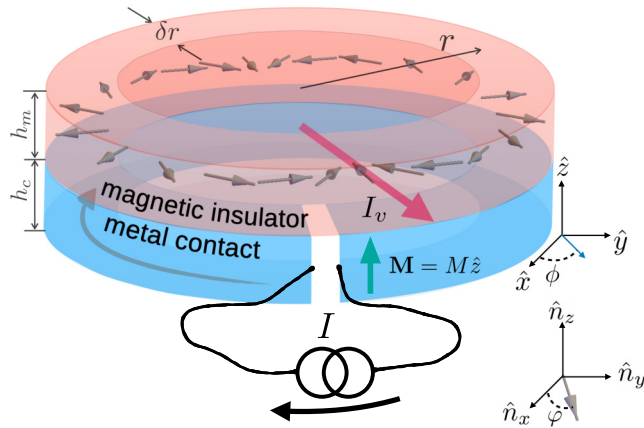


FIG. 1. The ring-shaped bilayer with a radius r , width δr , and heights h_m for the magnetic insulator and h_c for the metal contact. The order parameter of this magnetic insulator with easy- xy -plane anisotropy is parametrized by the spin-space azimuthal angle φ . The (ferromagnetic) metal layer has a uniform magnetization $\mathbf{M} = M\hat{z}$ and an azimuthal current I . The electric current induces a vortex flow I_v in the radial direction, which builds up an azimuthal winding density $\partial_t\varphi$ of the magnetic order parameter, where $l (= r\phi$ in polar coordinates) is the polar position in the plane of the annulus.

by Stokes theorem, is also the total winding number at the boundary $\partial\Omega$. Here \mathbf{n}_{\parallel} is the easy-plane projection of the order parameter \mathbf{n} . We remark that this construction is true not only at the low-temperature regime, where \mathcal{N} is integer valued, but also applicable at high temperatures and the paramagnetic regime (even in the lattice limit [22]), where the vortex number is not quantized.

To load the free energy associated with the magnetic winding texture, we operate the magnetic system near the Curie temperature (paramagnet regime) so that vortices and antivortices deconfine to form a two-dimensional, two-component plasma with finite vortex conductivity σ_v [21]. A constant electric current I circulating in the magnetic metal contact (see Fig. 1) energetically biases a radial vortex flow I_v [21] based on symmetry analysis. The electric current and vortex current are Magnus cross-coupled, as shown in Fig. 2(a). We articulate the detailed mechanism in a later section.

Using this externally driven vortex flow, we are able to reverse the typical “phase-slip” process in superfluids [5,23,24] and build up a finite order-parameter winding density $\partial_t\varphi$ in the magnetic insulator. The rate of change of the magnetic winding number and the intensity of the vorticity flow are related by the conservation law for the vortex 3-current (1):

$$d\mathcal{N}/dt = I_v. \quad (3)$$

As the winding number accumulates, the magnetic configuration builds up a finite free-energy and exerts a restoring force on the vortex flow, which decays exponentially and eventually vanishes when the restoring force balances the external drive. This type of process is analogous to the experimental proposal by Pearl [25], in which a magnetic screw rotating inside a superconducting cylinder is used to propagate vortices radially in order to increase the azimuthal superflow. In this

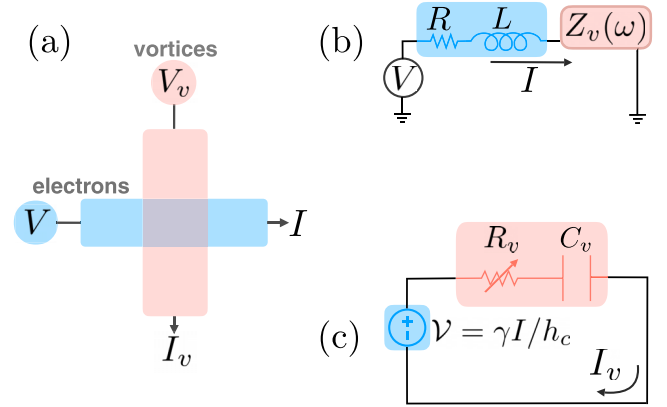


FIG. 2. (a) Schematic in Fig. 1 shows two viscously coupled hydrodynamic entities: one is electron flow I and the other is vortex flow I_v . The electrical circuit (b) has a current I , resistance R , self-inductance L (due to geometry), and effective impedance $Z_v(\omega)$ arising from the vortex-flow backaction on the electric circuit. Within the vortex circuit (c), the electric current I acts as a bias $\mathcal{V} = \gamma I/h_c$ for the vortex flow, where γ/h_c parametrizes the Magnus force between the electron and vortex degrees of freedom. Vortex flow through the magnetic bulk experiences resistance R_v , which is temperature dependent. The accumulated magnetic texture stores energy according to the capacitance C_v .

system, the mechanical energy of the rotating magnetic screw is converted into the energy associated with the increased winding of the order parameter. Similarly, our system converts electrical energy into the exchange energy of the magnetic texture.

Tuning the temperature for our magnetic system well below the Curie temperature T_c keeps the winding texture within plane, due to the easy-plane anisotropy, thus endowing it with topological protection. In this regime, the conductivity of vortices and hence the unwinding process is exponentially suppressed. As a result, the energy associated with the magnetic texture can be stored indefinitely in the absence of an external drive. To release the energy stored in the magnetic winding texture, we can simply raise the temperature near T_c and make use of the natural vortex flow in the “phase-slip” regime. The electromotive force from the vortex flow becomes the output voltage of the magnetic battery.

Main results. As we explain below, the dynamics of the system in Figs. 1 and 2 can be understood by mapping to two coupled circuits, one for electron flow and the other for topological charge (vortex) flow. For the topological charge circuit [see Fig. 2(c)], the electric current I in the metal contact plays the role of a bias, which applies the vortex-motive force $\gamma I/h_c$, triggering a vortex current I_v . Here γ/h_c is an interfacial spin-transfer torque parameter to be defined below. The magnetic insulator itself behaves like a vortex capacitor (C_v) and resistor (R_v) in series.

For the electric circuit, a reciprocal electromotive force $\mathcal{E}_{\text{EMF}} = \gamma I_v/h_c$ arises from the coupling between electron and vortex dynamics [26,27], in series with the resistance R and the magnetic inductance L of the metal contact. The Onsager reciprocity [28] between the two circuits can be expressed in

the compact form $\mathbf{V} = \hat{\mathcal{R}}\mathbf{I}$. In our treatment, the geometric inductance L may be neglected (as shown below). Ohms law then becomes,

$$\begin{pmatrix} V \\ V_v \end{pmatrix} = \begin{pmatrix} R & \gamma/h_c \\ -\gamma/h_c & R_v \end{pmatrix} \begin{pmatrix} I \\ I_v \end{pmatrix}, \quad (4)$$

where V is the electric voltage drop across the metallic contact and $V_v = -Q/C_v$ is the effective chemical potential associated with the accumulated topological charge $Q \equiv 2\pi\mathcal{N}$ ¹ the resistance matrix $\hat{\mathcal{R}}$ is positive semi-definite and time reversal antisymmetric. We will see that the electromotive force results in an impedance in the electric circuit, interpolating between a resistance (in the high-frequency response, compared with the characteristic $R_v C_v$ time) and an inductance (at low frequencies). As we discuss below, this inductance can exceed the geometrical inductance within the electrical circuit, leading us to propose to experimentally characterize the vorticity-current interaction through its contribution to the effective inductance.

Lastly, by neglecting the geometric inductance L , we estimate the charging efficiency, defined to be the ratio of the total energy stored to the total energy input, to be

$$\eta = \frac{1/2}{RR_v h_c^2 / \gamma^2 + 1}, \quad (5)$$

from which we see explicitly that the efficiency benefits from a thinner metal contact h_c . The three parameters (R , R_v , and γ/h_c) correspond to three dissipation channels: electrical resistance of the metal, resistance of the vortex current in the magnetic insulator, and their mutual resistance, respectively.

Biased vortex flow. A motive bias for vortex flow is established by a circulating electric current I (see Fig. 1) in a magnetically polarized metal contact ($\mathbf{M} = M\hat{\mathbf{z}}$). This current exerts a long-wavelength torque (per unit area) on the magnetic texture [21],

$$\boldsymbol{\tau} = \frac{\gamma n_z}{\pi} (\vec{j} \cdot \vec{\nabla}) \mathbf{n}, \quad (6)$$

where $j = I/h_c \delta r$ is the azimuthal electric current density, and n_z is the z component of the magnetic order parameter. $\gamma \equiv \text{sgn}(M) \pi \hbar h_{\text{eff}}/e$, where the length scale h_{eff} can be loosely interpreted as the spatial extent of the torque (proximity effect at the interface) within the insulator. The torque does work upon magnetic dynamics at the rate

$$\dot{W} = \int dxdy \boldsymbol{\tau} \cdot (\mathbf{n} \times \dot{\mathbf{n}}) = \gamma \int dxdy (\vec{\mathcal{J}} \times \vec{j}) \cdot \hat{\mathbf{z}}, \quad (7)$$

where the integration is performed over the interface. Here, we have taken, for simplicity, the magnitude of the order parameter to be fixed, $\mathbf{n} = 1$. In the high-temperature regime, where \mathbf{n} is fluctuating strongly, a similar result is expected, albeit with a renormalized prefactor. Equation (7) indicates that the coupling between electron and vortex dynamics is Magnus crosslike [see Fig. 2(a)]. In other words, the electric current tangential to a magnetic interface produces a Magnus

force on vortices, resulting in a transverse vortex flow, and vice versa. This underlies the mechanism for building up and relaxing the winding texture in the magnetic insulator.

Mapping onto two coupled circuits. We first consider the vortex dynamics in the magnetic insulator by exploiting the duality between the XY magnet and electrostatics in two dimensions [29,30]. In the low-temperature regime (for simplicity), \mathbf{n} is in plane and has a fixed magnitude (though, the results we obtain also generalize to the high-temperature regime where the magnitude of \mathbf{n} is allowed to fluctuate). The duality is accomplished by identifying the total winding of the magnetic order parameter, multiplied by 2π , with the electric charge $Q = 2\pi\mathcal{N}$, and the spatial gradients of the order-parameter angle with the electric field $\vec{E} = \mathcal{A} \vec{\nabla} \varphi \times \hat{\mathbf{z}}$, where \mathcal{A} is the order-parameter stiffness. We can now recast the definition of the winding number (2) as Gauss's law for the electric charge $\int d\vec{s} \cdot \vec{E} = Q/\epsilon$, where $d\vec{s} = d\vec{l} \times \hat{\mathbf{z}}$ is the line element in the radial direction and $\epsilon = 1/\mathcal{A}$ is the permittivity. Mapping the energy expression for the insulating magnet to electrostatic notation gives

$$\mathcal{E} = h_m \frac{\mathcal{A}}{2} \int dxdy (\vec{\nabla} \varphi)^2 = h_m \int dxdy \frac{\epsilon \vec{E}^2}{2}, \quad (8)$$

where h_m is the height of the magnetic insulator.

Therefore, driving topological charges (vortices) from the inner edge to the outer edge can be interpreted as a charging-capacitor process, which is triggered by a charge transfer (that is linked to the winding number) across the annulus. Noting that the power (7) can be rewritten as $\dot{W} = \gamma I I_v / h_c$, we can view the metallic contact as a battery with voltage $\mathcal{V} = \gamma I / h_c$ acting on a vortex $R_v C_v$ circuit, as illustrated in Fig. 2. The effective capacitance can be extracted by simply equating the energy (8) with $\mathcal{E} = Q^2 / 2C_v$, whereas Ohm's law [31] $\vec{\mathcal{J}} = -\sigma_v \vec{\nabla} \mu$ gives the resistance $R_v = \Delta\mu / I_v$, where $I_v = 2\pi r \mathcal{J}$ is the vortex current and $\Delta\mu$ is the motive force on the vortex flow. Thus we arrive at the effective vortex capacitance and resistance

$$C_v = \frac{1}{\mathcal{A}} \frac{2\pi r}{h_m \delta r}, \quad R_v = \frac{1}{\sigma_v} \frac{\delta r}{2\pi r}. \quad (9)$$

Here σ_v^{-1} is the vortex resistivity whose main contributions arise from vortex collisions (such as umklapp scattering, disorder, etc.) and Gilbert damping.

The vortex current acts reciprocally on the electric circuit, as summarized in Eq. (4), from which we wish to determine its effective impedance in the electric current. After Fourier transforming and solving for the electric response, we arrive at the total impedance:

$$Z(\omega) \equiv \frac{V(\omega)}{I(\omega)} = R + i\omega L + \frac{i\omega C_v \gamma^2 / h_c^2}{1 + i\omega R_v C_v}, \quad (10)$$

where the last term [henceforth denoted $Z_v(\omega)$] is the vorticity impedance, arising from the coupling between electron and vortex dynamics. In the high-frequency regime ($\omega \gg 1/\tau$), where $\tau = R_v C_v$ is the timescale of the vortex charging (or discharging) process, one obtains $Z_v(\omega) = \gamma^2 / h_c^2 R_v$, indicating that the magnetic insulator, generating an electromotive force against the input electric current, behaves like a resistor in the electric circuit. In the opposite regime where $\omega \ll 1/\tau$,

¹Note that the resistance matrix $\hat{\mathcal{R}}$ is antisymmetric since the metallic magnetization flips sign under time reversal (when one invokes Onsager reciprocity). One can also easily check the positive-definiteness of the dissipation $\mathbf{I}^T \cdot \mathbf{V} \geq 0$.

we have $Z_v(\omega) = i\omega C_v \gamma^2 / h_c^2$, suggesting that the magnetic insulator plays the role of an inductor with $L_v = C_v \gamma^2 / h_c^2$.

Battery efficiency and quantitative estimates. The dc electric current I flowing in the metal contact (Fig. 1) eventually results in a steady-state magnetic texture, with winding density $\partial_t \varphi = \gamma I / \mathcal{A} h_c h_m \delta r$ and an associated free energy,

$$\mathcal{E} = \frac{1}{2} C_v \mathcal{V}^2 = \frac{1}{\mathcal{A}} \frac{\pi r}{h_m \delta r} \left(\frac{\gamma I}{h_c} \right)^2, \quad (11)$$

at time $t \gg \tau = R_v C_v = 1 / \mathcal{A} \sigma_v h_m$. Here the vortex conductivity $\sigma_v = \rho_v \mu = \rho_v D / k_B T$ depends on the temperature through the free-vortex density ρ_v and vortex mobility μ (via the Einstein relation). In the extreme limit $T \ll T_c$, where $\rho_v \sim 0$, we have zero vortex conductivity, leading to $\tau \rightarrow \infty$. In the opposite regime (above the Curie temperature $T_c \sim J / k_B$), the order parameter varies on the atomic scale, $\rho_v \sim 1 / a^2$ and $D \sim J a^2 / \hbar$, giving the lower bound of the charging time $\tau \sim \hbar / J$. Thus the vortex conductivity σ_v and τ are highly tunable by temperature.

To estimate the efficiency η of the charging process, we neglect the geometrical inductance of the metal contact and allow the device to charge for a time τ . The charging will be accomplished by using a single square-wave pulse of current I . The total external energy input during the charging process is

$$\mathcal{W} = \int_0^\tau dt IV(t) = I^2 R \tau + \tau \frac{\mathcal{V}^2}{R_v} (1 - e^{-1}), \quad (12)$$

where $V(t)$ is the electric voltage drop across the metal contact that can be obtained by solving Eq. (4). These terms take into account the energy loss due to Joule heating and vortex motion as well as the stored energy within the magnetic texture. The numerical factor of the second term is of order unity; replacing this factor with 1 leads to the efficiency defined in Eq. (5) of the charging process. Considering the regime where $\tau \sim \hbar / J$, we have $RR_v h_c^2 / \gamma^2 \sim h_m h_c / h_{\text{eff}}^2 k_F^2 a d$, where d and k_F are the mean free path and Fermi wave number of electrons within the metal, respectively. It is clear that the efficiency benefits from improving the conducting quality of the metal and decreasing thicknesses of both insulating magnet and metallic contact, which makes sense intuitively. When taking the geometrical inductance L into account we can improve the efficiency further. In the limiting case of $L \rightarrow \infty$, where the charging process is adiabatic, the efficiency can, in principle, approach 1.

The maximal energy-storage capacity, another quantity of interest, is dictated by the Landau criterion for energetic stability [32], where the magnetic texture is maximally wound. It is achieved when the winding texture energy $[\sim \mathcal{A} (\partial_t \varphi)^2]$ is comparable to the easy-plane anisotropy energy ($\sim \mathcal{K}$) that fixes the winding within the easy plane. Let us take the bulk stiffness to be $\mathcal{A} = 5 \times 10^{-12}$ J/m, an easy-plane anisotropy strength of $\mathcal{K} = 5 \times 10^5$ J/m³, and mass density 5.11 g/cm³ (yttrium iron garnet), which yields for the winding density $1 / \partial_t \varphi = \sqrt{\mathcal{A} / \mathcal{K}} \sim 3$ nm and a specific energy density of 0.1 J/g. Such an energy can be loaded by applying an electric current density of 10^{12} A/m² within a thin metal contact, which is feasible experimentally [8]. We can further increase the specific energy density by enhancing the easy-plane anisotropy. For example, in the extreme limit where the order parameter

can vary on the atomic scale, $1 / \partial_t \varphi \sim a$, we have the specific energy density 10^4 J/kg, which is about an order of magnitude below the capacity of lithium-ion batteries.

To characterize the vorticity-current interaction, which underlies the mechanism of our proposal, we suggest measuring its contribution to the electric inductance in the rf response. To this end, we note that L_v can be manufactured to exceed with the geometrical inductance L : $L_v / L \sim e^2 a / \alpha^2 J h_m \delta r \sim 1$ (where α is the fine structure constant), when we take used $\delta r h_m \sim 100$ nm². Alternatively, one can measure the (transient) vortex discharging process, where the electric voltage of the metal is $V(t) = V_{\text{max}} e^{-t/\tau}$, by solving Eq. (4) with an open electric circuit. For a thin contact ($h_c \sim h_{\text{eff}}$), one obtains that $V_{\text{max}} \tau \sim \hbar r / e \sqrt{\mathcal{A} / \mathcal{K}}$. Assuming $r \sim 1$ μ m and $\tau \sim 10$ ns, which should be easily accessed experimentally, we get a measurable voltage drop of $V_{\text{max}} \sim 10^{-4}$ V.

Summary and outlook. We have proposed an experimentally feasible energy-storage concept in insulating magnets based on the collective transport of vortices emerging out of the topologically nontrivial real-space order-parameter textures. This allows us to utilize the current-magnet interaction with a focus on the dynamics of topological textures rather than the conventional spin currents. The energy associated with the winding texture can be loaded by electric means, which biases vortex flow within the magnet [21,22]. The system is mapped onto two coupled circuits, where we interpret the energy-loading process as a capacitor-charging action. This energy storage is attractive due its potential longevity [33,34], endowed by the topological nature of vorticity, and its compatibility with integrated spintronic circuits [6,10–12] and quantum-information processes based on insulating magnets [18–20].

Note that the heating/cooling in the vicinity of T_c (which may be a natural consequence of the Joule heating by the applied current) is invoked in our proposal only to change the vorticity transport parameters, which effectively undergo a transition between diffusive (above T_c) and insulating (below T_c) behaviors. The associated dissipation of energy (by Joule heating) is accounted for in our analysis and would not be of much concern otherwise if the vortex conductivity changes significantly over a small temperature range. Other ways to modulate the impedance of vorticity may, in principle, be developed in the future.

One could envision a variety of generalizations of our proposal by exploiting different topological hydrodynamics. An immediate example is the magnetic hedgehog in three dimensions [35]. When a hedgehog passes through a chiral magnet [36], a finite skyrmion density is built up which is associated with finite energy and can be devised to store energy. The resultant skyrmion density is protected by Dzyaloshinskii-Moriya interaction, which plays a role of easy-plane anisotropy for winding texture. We remark that this is the generic property of n -dimensional nonlocal topological defects, which would establish $(n - 1)$ -dimensional nonlinear textures when they flow through a medium, dictated by the generalized Stokes' theorem. Other types of topologically conserved local defects, such as skyrmions in two-dimensional magnetic films [37] and three-dimensional skyrmionic textures in frustrated magnets [38], can also

be quite valuable potentially for energy-storage purposes. These systems provide ample opportunities to explore energy-storage concepts based on spin degrees of freedom and deserve further investigation.

Acknowledgments. We are grateful to Mostafa Ahari, Wei Han, and Jiang Xiao for insightful discussions. This work was supported by the US Department of Energy, Office of Basic Energy Sciences, under Award No. DE-SC0012190.

-
- [1] *Spin Current*, edited by S. Maekawa, S. O. Valenzuela, E. Saitoh, and T. Kimura, Series on Semiconductor Science and Technology (Oxford University Press, Oxford, England, 2015).
- [2] Y. Tserkovnyak, *J. Appl. Phys.* **124**, 190901 (2018).
- [3] H. Ochoa and Y. Tserkovnyak, *Int. J. Mod. Phys. B* **33**, 1930005 (2019).
- [4] Y. Tserkovnyak and J. Xiao, *Phys. Rev. Lett.* **121**, 127701 (2018).
- [5] S. K. Kim and Y. Tserkovnyak, *Phys. Rev. Lett.* **116**, 127201 (2016); S. K. Kim, S. Takei, and Y. Tserkovnyak, *Phys. Rev. B* **93**, 020402(R) (2016).
- [6] D. A. Allwood, G. Xiong, C. C. Faulkner, D. Atkinson, D. Petit, and R. P. Cowburn, *Science* **309**, 1688 (2005).
- [7] A. Fert, V. Cros, and J. Sampaio, *Nat. Nanotechnol.* **8**, 152 (2013).
- [8] S. S. P. Parkin, M. Hayashi, and L. Thomas, *Science* **320**, 190 (2008).
- [9] A. Fert, *Rev. Mod. Phys.* **80**, 1517 (2008).
- [10] A. V. Chumak, V. I. Vasyuchka, A. A. Serga, and B. Hillebrands, *Nat. Phys.* **11**, 453 (2015).
- [11] A. Khitun, M. Bao, and K. L. Wang, *J. Phys. D* **43**, 264005 (2010).
- [12] J. Lan, W. Yu, R. Wu, and J. Xiao, *Phys. Rev. X* **5**, 041049 (2015).
- [13] S. Zhang and Y. Tserkovnyak, [arXiv:2003.11058](https://arxiv.org/abs/2003.11058) [Phys. Rev. Lett. (to be published)].
- [14] J. Grollier, D. Querlioz, and M. D. Stiles, *Proc. IEEE* **104**, 2024 (2016).
- [15] K. Yue, Y. Liu, R. K. Lake, and A. C. Parker, *Sci. Adv.* **5**, eaau8170 (2019).
- [16] J. Torrejon, M. Riou, F. A. Araujo, S. Tsunegi, G. Khalsa, D. Querlioz, P. Bortolotti, V. Cros, K. Yakushiji, A. Fukushima, H. Kubota, S. Yuasa, M. D. Stiles, and J. Grollier, *Nature (London)* **547**, 428 (2017).
- [17] A. Sengupta and K. Roy, *Appl. Phys. Express* **11**, 030101 (2018).
- [18] S. Takei, Y. Tserkovnyak, and M. Mohseni, *Phys. Rev. B* **95**, 144402 (2017).
- [19] J. Zou, S. K. Kim, and Y. Tserkovnyak, *Phys. Rev. B* **101**, 014416 (2020).
- [20] A. Kamra, E. Thingstad, G. Rastelli, R. A. Duine, A. Brataas, W. Belzig, and A. Sudbø, *Phys. Rev. B* **100**, 174407 (2019).
- [21] J. Zou, S. K. Kim, and Y. Tserkovnyak, *Phys. Rev. B* **99**, 180402(R) (2019).
- [22] Y. Tserkovnyak and J. Zou, *Phys. Rev. Research* **1**, 033071 (2019).
- [23] S. M. Girvin and K. Yang, *Modern Condensed Matter Physics*, 1st ed. (Cambridge University Press, Cambridge, England, 2019).
- [24] B. I. Halperin, G. Refael, and E. Demler, *Int. J. Mod. Phys. B* **24**, 4039 (2010).
- [25] J. Pearl, Vortexes are creating a stir in the superconductor field, *Electronics (USA)*, 1966, Vol. 39, p. 100.
- [26] G. E. Volovik, *J. Phys. C: Solid State Phys.* **20**, L83 (1987).
- [27] C. H. Wong and Y. Tserkovnyak, *Phys. Rev. B* **80**, 184411 (2009).
- [28] L. Onsager, *Phys. Rev.* **37**, 405 (1931).
- [29] J. M. Kosterlitz, *J. Phys. C* **7**, 1046 (1974).
- [30] S. Dasgupta, S. Zhang, I. Bah, and O. Tchernyshyov, *Phys. Rev. Lett.* **124**, 157203 (2020).
- [31] L. P. Pitaevskii and E. Lifshitz, *Physical Kinetics*, Course of Theoretical Physics Vol. 10 (Butterworth-Heinemann, Oxford, England, 1981).
- [32] E. B. Sonin, *Adv. Phys.* **59**, 181 (2010).
- [33] A. J. Smith, J. C. Burns, S. Trussler, and J. R. Dahn, *J. Electrochem. Soc.* **157**, A196 (2010).
- [34] D. Apalkov, B. Dieny, and J. M. Slaughter, *Proc. IEEE* **104**, 1796 (2016).
- [35] J. Zou, S. Zhang, and Y. Tserkovnyak, [arXiv:2006.10910](https://arxiv.org/abs/2006.10910).
- [36] P. Milde, D. Köhler, J. Seidel, L. M. Eng, A. Bauer, A. Chacon, J. Kindervater, S. Mühlbauer, C. Pfleiderer, S. Buhrandt, C. Schütte, and A. Rosch, *Science* **340**, 1076 (2013).
- [37] H. Ochoa, S. K. Kim, and Y. Tserkovnyak, *Phys. Rev. B* **94**, 024431 (2016).
- [38] R. Zarzuela, H. Ochoa, and Y. Tserkovnyak, *Phys. Rev. B* **100**, 054426 (2019).